Pergamon

0301-9322(93)E0035-4

Int. J. Multiphase Flow Vol. 20, No. 2, pp. 397–414, 1994

0301-9322/94 $7.00 + 0.00

CONVECTION IN MULTIPLE LAYERS OF IMMISCIBLE LIQUIDS IN A SHALLOW CAVITY—II

STEADY THERMOCAPILLARY CONVECTION

A. PRAKASH and J. N. KOSTER†

Department of Aerospace Engineering Sciences, University of Colorado, Campus Box 429, Boulder, CO 80309, U.S.A.

(Received 23 November 1992; in revised form 12 August 1993)

Abstract—The problem of thermocapillary convection in multiple immiscible liquid layers in a differentially heated shallow rectangular cavity with rigid and insulated upper and lower boundaries is considered. A three-layer system is considered as a model for multiple liquid layers. The middle layer is encapsulated on both sides by immiscible liquids, and features two interfaces which are considered to be deformable. The method of matched asymptotic expansions is used to determine the flow in the two distinct regions: the core region characterized by parallel flow; and the end-wall regions where flow turns around. Interfacial tension gradients induced by differential heating of the cavity drive the flow. Mechanical coupling across interfaces between immiscible liquids is investigated by varying the encapsulant viscosity and the height of encapsulant layers.

Key Words: thermocapillary convection, multiple immiscible layers, asymptotic theory

INTRODUCTION

In part I of this series of papers (Prakash & Koster 1994, this issue, pp. 383–396) the effects of buoyancy on multiple immiscible layers were studied and thermocapillary effects were excluded. As the genesis of buoyancy is gravity, in the low-gravity environment aboard a spacecraft buoyancy-induced convection can be significantly reduced. To take advantage of this environment, space processing of GaAs utilizing the liquid encapsulated float zone technique has been proposed (Barocela & Jalilevand 1987). Low gravity is, however, not a panacea for eliminating convective flow. A significant source of convection in low-gravity environments is thermocapillary convection, which results from the change of surface tension with temperature.

Thermocapillary convection in multiple liquid layers is an extension of the convection problem in a single layer confined in a differentially heated cavity, which is either completely confined or features a free surface. Levich (1962) and Birikh (1966) performed the earliest analytical investigations of steady thermocapillary convection in unbounded liquid layers.

For shallow cavities, with height much smaller than length (aspect ratios $d/l \ll 1$), direct numerical modeling of the flow is expensive. However, analytical progress is possible with asymptotic methods, as demonstrated by Cormack *et al.* (1974)—hereafter referred to as CLI—for natural convection and by Sen & Davis (1982)—hereafter referred to as S&D—for thermocapillary convection. Both CLI and S&D present a theory that is valid for shallow cavities ($d/l \ll 1$) in the asymptotic limit of negligible aspect ratio ($A \to 0$). Both CLI and S&D show that convective flow in a shallow rectangular cavity can be divided into three, horizontally adjacent regions: the central, or "core", region; and the two end regions where flow turns around.

S&D utilize an analysis that is analogous to CLI's theory to analyze flow in a liquid layer under low-gravity conditions, where convection is due to thermocapillary forces only and buoyancy effects are neglected. They include the complicating effects of deformable interfaces and liquid–solid contact angles.

†Author for correspondence.

Three immiscible layers are considered to be representative of a multilayer system. A one-dimensional solution, based on the analysis of Villers & Platten (1990), for a free–free layer was presented previously by the authors (Prakash *et al.* 1993).

The multilayer problem is characterized by mechanical and thermal coupling across liquid interfaces. Mechanical coupling occurs via the transfer of momentum across interfaces. The momentum generated by interfacial tension gradients is transferred to the adjoining layers via continuity of the interfacial tangential velocity and the balance of shear stress across the interface. Together these two conditions comprise the "no-slip" condition at liquid–liquid interfaces. Prakash & Koster (1993) presented a one-dimensional model of this problem which included mechanical coupling across the interfaces. Fontaine & Sani (1992), as well as Doi & Koster (1993), presented a numerical simulation of the case of a free double layer with a strong surface tension and weaker interface tension gradient.

Here we utilize S&D's asymptotic theory to study steady thermocapillary convection in multiple immiscible liquid layers, driven by two "equal" strength interface tension gradients, while excluding the influence of buoyancy. In this investigation, the interfaces are assumed to be pinned at the solid boundaries. It is the mechanical and thermal coupling that distinguishes this analysis from that of S&D.

MATHEMATICAL FORMULATION

We consider the fluid dynamics of a system of three immiscible liquid layers in a shallow, rectangular, two-dimensional cavity of aspect ratio $d/l \ll 1$. The cavity has length l, and d is the height of the middle layer. The three layer heights are not necessarily equal. However, they are all of the same order and each layer aspect ratio is considered small. The cavity height is, therefore, of order $3d$, which is considered to be much smaller than the cavity length. The cavity is differentially heated from the side, while the top and bottom boundaries are rigid and thermally insulated. A sketch of the geometry being considered is shown in figure 1. Horizontal differential heating produces a temperature gradient parallel to the two interfaces. As interfacial tension is a function of temperature, the imposed temperature gradient produces interfacial tension gradients. The interfacial tension gradients induce fluid flow, which is commonly referred to as thermocapillary or Marangoni convection.

Governing Equations

Utilizing the stream function–vorticity formulation of the Navier–Stokes equations, the non-dimensional governing equations of fluid flow in each liquid layer [i = t (top), m (middle) or b (bottom)] are:

$$\nu^i[\psi^i_{yyyy} + 2A^2\psi^i_{xxyy} + A^4\psi^i_{xxxx}] = \mathrm{Re}\, A\{[\psi^i_y\psi^i_{xyy} - \psi^i_x\psi^i_{yyy}] + A^2[\psi^i_y\psi^i_{xxx} - \psi^i_x\psi^i_{xxy}]\} \qquad [1]$$

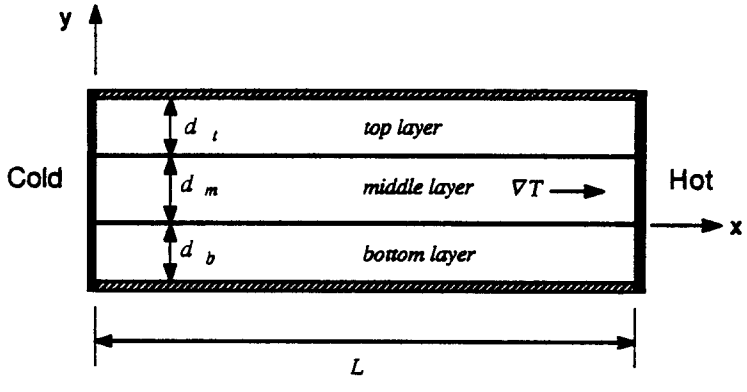

Figure 1. Sketch of the shallow cavity with three immiscible liquid layers.

and

$$\kappa^i[\theta^i_{yy} + A^2\theta^i_{xx}] = \mathrm{M}A[\psi^i_y\theta^i_x - \psi^i_x\theta^i_y]. \quad [2]$$

For a detailed derivation of these equations we refer to S&D. The governing equations have been scaled using the thermophysical properties of the middle layer, the middle-layer height d, the length of the cavity l, the applied temperature differences ΔT, the average temperature T_0 and the interfacial tension gradient γ of the lower interface. The following length, velocity, temperature and pressure scales are used:

$$x^* = lx; \quad y^* = dy \quad [3]$$

and

$$u^* = \left(\frac{\gamma\Delta T}{\mu}\right)\left(\frac{d}{l}\right)u; \quad T^* = T_0 + \Delta T\theta; \quad p^* = \frac{\mu u^* L}{d^2}. \quad [4]$$

The non-dimensional parameters appearing in the above formulation are also based on the middle-layer thermophysical properties, the middle-layer height d, the cavity length l, the lower interfacial tension σ_0 and the interfacial tension gradient γ as follows

$$A = \frac{d}{l}; \quad \mathrm{Pr} = \frac{\nu}{\kappa} \quad [5]$$

and

$$\mathrm{Re} \equiv \frac{u^* d}{\nu} = A\frac{\gamma\Delta T d}{\mu\nu}; \quad \mathrm{M} \equiv \frac{u^* d}{\kappa} = A\frac{\gamma\Delta T d}{\kappa\mu} = \mathrm{Re\,Pr}; \quad \mathrm{Ca} \equiv \frac{u^*\mu}{\sigma_0} = A\frac{\gamma\Delta T}{\sigma_0}, \quad [6]$$

where A is the aspect ratio, Pr is the Prandtl number, Re is the Reynolds number, M is the Marangoni number and Ca is the Capillary number. Capitalized superscripts denote ratios of the thermophysical properties of the top (t) and bottom (b) layers with respect to the middle (m) layer, i.e.

$$\nu^{\mathrm{B}} = \frac{\nu_{\mathrm{b}}}{\nu_{\mathrm{m}}}; \quad \nu^{\mathrm{T}} = \frac{\nu_{\mathrm{t}}}{\nu_{\mathrm{m}}}. \quad [7]$$

Ratios of other thermophysical properties and layer height ratios are denoted similarly. For the middle layer, the ratios are simply unity. Interfacial tensions and their temperature gradients are scaled using the lower interface values, as follows:

$$\gamma^{\mathrm{U}} = \frac{\gamma_{\mathrm{u}}}{\gamma}; \quad \sigma_0^{\mathrm{U}} = \frac{\sigma_{0_{\mathrm{u}}}}{\sigma_0}; \quad \gamma^{\mathrm{L}} = 1; \quad \sigma_0^{\mathrm{L}} = 1. \quad [8]$$

Also, interfacial deformations of the lower (l) and upper (u) interfaces are scaled using the middle-layer height d:

$$h^{\mathrm{L}}(x) = \frac{h_{\mathrm{l}}(x)}{d}; \quad h^{\mathrm{U}}(x) = \frac{h_{\mathrm{u}}(x)}{d}. \quad [9]$$

At the four rigid walls the boundary condition is the no-slip condition. At the cold and hot end walls an isothermal condition applies, while at the insulated top and bottom boundaries a zero heat-flux condition applies. These conditions are:

$$\text{at } x = \mp 1/2, \qquad \psi^i = \psi^i_x = 0; \quad \theta^i = \mp 1/2; \quad h^j(x) = 0, \quad [10]$$

$$\text{at } y = -d^{\mathrm{B}}, \qquad \psi^{\mathrm{b}} = \psi^{\mathrm{b}}_y = 0; \quad \theta^{\mathrm{b}}_y = 0 \quad [11]$$

and

$$\text{at } y = 1 + d^{\mathrm{T}}, \qquad \psi^{\mathrm{t}} = \psi^{\mathrm{t}}_y = 0; \quad \theta^{\mathrm{t}}_y = 0. \quad [12]$$

For a detailed derivation of boundary conditions at the interfaces we again refer to S&D. Note that the interfaces are pinned at the side walls at fixed height. This assumption is based on experimental conditions of a forthcoming space-flight experiment, where the contact lines of the interfaces are pinned mechanically to the side walls by a knife-edge design. At the interfaces the

boundary conditions are continuity of velocity and temperature, the kinematic condition, balance of normal and shear stress and heat flux balance, these take the form:

at $y = h^{L}, 1 + h^{U}$,

$$\psi_x^{-j} = \psi_x^{+j}; \quad \psi_y^{-j} = \psi_y^{+j}, \tag{13}$$

$$\psi_x^{-j} + h_x^j \psi_y^{-j} = \psi_x^{+j} + h_x^j \psi_y^{+j} = 0, \tag{14}$$

$$-\langle p \rangle + \frac{2A^2}{(1 + A^2 h_x^{j2})} \langle \mu[(-\psi_{xy} - h_x^j \psi_{yy}) + A^2 h_x^j (h_x^j \psi_{xy} + \psi_{xx})] \rangle$$

$$= \frac{h_{xx}^j}{A\bar{C}(1 + A^2 h_x^{j2})^{3/2}} (\sigma_0^j - A^3 \bar{C} \gamma^j \theta^i), \tag{15}$$

$$\langle \mu[(1 - A^2 h_x^{j2})(\psi_{yy} - A^2 \psi_{xx}) - 4A^2 h_x^j \psi_{xy}] \rangle = -\gamma^j (1 + A^2 h_x^{j2})^{1/2} (\theta_x^j + h_x^j \theta_y^j) \tag{16}$$

and

$$\langle \lambda[\theta_y - A^2 h_x^j \theta_x] \rangle = 0, \tag{17}$$

where the operator $\langle\ \rangle$ is defined as

$$\langle f \rangle = f^{-j} - f^{+j} \tag{18}$$

and the superscripts $+j$ and $-j$ refer to liquids above and below interface j (l = lower, u = upper). Additionally, we have the conservation conditions:

at $y = h^{L}, 1 + h^{U}$,

$$\psi^{-j} = \psi^{+j} = 0 \tag{19}$$

and

$$\int_{-1/2}^{1/2} h^j(x)\, dx = 0. \tag{20}$$

To proceed further with the asymptotic expansion, an estimate of the order of the non-dimensional parameters characterizing the flow (Re, M and Ca) is required. We continue with S&D's development and also assume the flow to be "slow", i.e. both Re and M are small:

$$\mathrm{Re} = \overline{\mathrm{Re}}\, A; \quad \mathrm{M} = \overline{\mathrm{M}}\, A; \quad \mathrm{Ca} = \overline{\mathrm{Ca}}\, A^4, \tag{21}$$

where

$$\overline{\mathrm{Re}} \sim \overline{\mathrm{M}} \sim \overline{\mathrm{Ca}} \sim O(1); \quad \mathrm{Pr} \sim O(1). \tag{22}$$

The above limitation on Ca is discussed by S&D. This poses a rather severe limitation on the analysis, as the Pr of several liquids of interest in our experimental efforts is an order-of-magnitude or more larger than $O(1)$. Nevertheless, we proceed despite this restriction and leave the consideration of larger Pr for a future study.

The objective now is to solve the above system of equations in each of the three layers with applicable boundary conditions in the limit $A \to 0$.

Flow in the Core Region

In the core region, away from the end walls, flow streamlines are presumed to be nearly parallel to the interfaces. Vertical velocities in this region are considered to be very small in comparison with the horizontal velocities, ($v \sim Au$). The stream function in layer i (t = top, m = middle, b = bottom) is expanded using the small geometric parameter A as follows:

$$\psi^i = \psi_0^i + A\psi_1^i + A^2 \psi_2^i + \cdots. \tag{23}$$

Temperature and vorticity in the three layers are expanded in a similar fashion. The two interface deformations at interface j (l = lower, u = upper) are expanded using the small geometric parameter A as follows:

$$h^j = Ah_1^j + A^2 h_2^j + \cdots. \tag{24}$$

The interface is considered to be flat at $O(1)$.

Solution at O(1)

Upon substitution of the field variable expansions into the governing equations, we obtain the following simple form $O(1)$:

$$\psi^i_{0_{yyyy}} = 0; \quad \theta^i_{0_{yy}} = 0; \quad P^i_{0_x} = \mu^i \psi^i_{0_{yyy}}. \tag{25}$$

The boundary conditions at the four walls are the same as [10]–[12]. At this order, the boundary conditions across the jth interface become:

at $y = 0, 1$,

$$\psi_0^{-j} = \psi_0^{+j} = 0; \quad \psi_{0_y}^{-1} = \psi_{0_y}^{+j} \tag{26}$$

and

$$-\langle p_0 \rangle = \frac{\sigma^j_0 h^j_{1_{xx}}}{\overline{\text{Ca}}}; \quad \langle \mu \psi_{0_{yy}} \rangle = -\gamma^j \theta^j_{0_x}; \quad \langle \lambda \theta_{0_y} \rangle = 0. \tag{27}$$

The solution of the above system of equations is

$$\psi^i_0 = A^i_0 y^3 + B^i_0 y^2 + C^i_0 y + D^i_0, \tag{28}$$

$$\theta^i_x = x \tag{29}$$

and

$$h^j_1(x) = -\frac{\overline{\text{Ca}}(\mu^{-j} A_0^{-j} - \mu^{+j} A_0^{+j})}{\sigma^j_0} x^3 + H^j_1 x^2 + H^j_2 x + H^j_3. \tag{30}$$

As the O(i) core flow is presumed to be parallel, the coefficients A^i_0, B^i_0, C^i_0 and D^i_0 are all independent of x, which dictates θ^i_0 to be linear function of x. These coefficients are determined by satisfying the boundary conditions on the stream function. This leads to a system of 12 linear equations with 12 unknown constants. The coefficients H^i_1, H^i_2 and H^i_3 in [30] are yet to be determined by matching with the end-region solution.

Solution at O(A)

At $O(A)$, the governing equations reduce to:

$$\psi^i_{1_{yyyy}} = 0; \quad \theta^i_{1_{yy}} = 0; \quad p^i_{1_x} = \mu^i \psi^i_{1_{yyy}}. \tag{31}$$

At the interfaces, the boundary conditions become:

at $y = Ah^{\text{L}}_1, 1 + Ah^{\text{U}}_1$,

$$\psi^{-1}_{1_x} + h^j_{1_x} \psi^{-1}_{0_y} = \psi^{+j}_{1_x} + h^j_{1_x} \psi^{+j}_{0_y} = 0 \tag{32}$$

$$\psi^{-j}_{1_x} = \psi^{+j}_{1_x}; \quad \psi^{-j}_{1_y} + h^j_1 \psi^{-j}_{0_{yy}} = \psi^{+j}_{1_y} + h^j_1 \psi^{+j}_{0_{yy}} \tag{33}$$

and

$$-\langle p_1 \rangle = \frac{\sigma^j_0 h^j_{2_{xx}}}{\overline{\text{Ca}}}; \quad \langle \mu[\psi_{1_{yy}} + h^j_1 \psi_{0_{yyy}}] \rangle = -\gamma^j \theta^j_{1_x}; \quad \langle \lambda \theta_{1_y} \rangle = 0. \tag{34}$$

The conservation of return flow condition is

$$\psi^{-j}_1 + h^j_1 \psi^{-1}_{0_y} = \psi^{+j}_1 + h^j_1 \psi^{+j}_{0_y} = 0. \tag{35}$$

This condition is the integrated form of the kinematic condition [32].

The solution of the above system of equations is:

$$\psi^{\text{b}}_1 = h^{\text{L}}_1(x)[A^{\text{b}}_1 y^3 + B^{\text{b}}_1 y^2 + C^{\text{b}}_1 y + D^{\text{b}}_1], \tag{36}$$

$$\psi^{\text{m}}_1 = h^{\text{L}}_1(x)[A^{\text{bm}}_1 y^3 + B^{\text{bm}}_1 y^2 + C^{\text{bm}}_1 y + D^{\text{bm}}_1] + h^{\text{U}}_1(x)[A^{\text{tm}}_1 y^3 + B^{\text{tm}}_1 y^2 + C^{\text{tm}}_1 y + D^{\text{tm}}_1], \tag{37}$$

$$\psi^{\text{t}}_1 = \text{h}^{\text{U}}_1(x)[A^{\text{t}}_1 y^3 + B^{\text{t}}_1 y^2 + C^{\text{t}}_1 y + D^{\text{t}}_1] \tag{38}$$

$$\theta^i_1 = 0 \tag{39}$$

$$h_2^{\mathrm{L}} = -\frac{6\,\overline{\mathrm{Ca}}}{\sigma_0^{\mathrm{l}}}\left[(\mu^{\mathrm{B}}A_1^{\mathrm{b}} - A_1^{\mathrm{bm}})\iiint h_1^{\mathrm{L}}(x)\,\mathrm{d}x - A_1^{\mathrm{tm}}\iiint h_1^{\mathrm{U}}(x)\,\mathrm{d}x\right] + K_1^{\mathrm{l}}x^2 + K_2^{\mathrm{l}}x + K_3^{\mathrm{l}} \quad [40]$$

and

$$h_2^{\mathrm{U}} = -\frac{6\,\overline{\mathrm{Ca}}}{\sigma_0^{\mathrm{u}}}\left[(A_1^{\mathrm{tm}} - \mu^{\mathrm{T}}A_1^{\mathrm{t}})\iiint h_1^{\mathrm{U}}(x)\,\mathrm{d}x + A_1^{\mathrm{bm}}\iiint h_1^{\mathrm{L}}(x)\,\mathrm{d}x\right] + K_1^{\mathrm{u}}x^2 + K_2^{\mathrm{u}}x + K_3^{\mathrm{u}}. \quad [41]$$

At this order of the solution, the flow in the middle layer is influenced by the upper and lower interfacial deformations. This leads to 4 additional constants, making a total of 16 constants to be evaluated by satisfying the boundary conditions on the stream function. Also, at this order, the interfacial deformations at both interfaces are mutually coupled. The constants appearing in the interfacial deformation equations are to be evaluated by matching with the end-region solution.

Solution at $O(A^2)$

At this order we consider only the temperature field, as this is needed to obtain the matching end-wall solution. At this order, the governing equation for temperature is

$$\theta_{2_{yy}}^i = \frac{\overline{\mathrm{M}}}{\kappa^i}\psi_{0_y}^i\theta_{0_x}^i \quad [42]$$

and the boundary conditions at the interfaces are:

at $= Ah_1^{\mathrm{L}} + A^2h_2^{\mathrm{L}},\ 1 + Ah_1^{\mathrm{U}} + A^2h_2^{\mathrm{U}}$,

$$\theta_2^{-i} = \theta_2^{+i}; \quad \langle\lambda\theta_{2_y}\rangle = 0. \quad [43]$$

The solution for the above equation is

$$\theta_2^i = \frac{\overline{\mathrm{M}}}{\kappa^i}\left(\frac{A_0^i}{4}y^4 + \frac{B_0^i}{3}y^3 + \delta_1^i y + \delta_2^i\right). \quad [44]$$

Coefficients A_0^i and B_0^i are the previously evaluated constants from the flow at $O(1)$, and the constants δ_1^i and δ_2^i are to be determined from the boundary conditions.

Flow in the End Regions

In the end-wall regions, not only must the wall boundary conditions be satisfied, the solution must also match the core flow away from the walls. To capture the flow pattern in the end regions, we stretch the coordinates in the vicinity of the cold and hot walls as follows:

$$\left\{\xi = \frac{\frac{1}{2}+x}{A}, \eta = y\right\}\left\{\chi = \frac{\frac{1}{2}-x}{A}, \zeta = y\right\}. \quad [45]$$

In the following development, without loss of generality, we concentrate on the cold-wall region. The governing equations in the stretched coordinate system become:

$$\nabla^4\psi^i = A\frac{\overline{\mathrm{Re}}}{\nu^i}[\psi_\eta^i(\psi_{\xi\eta\eta}^i + \psi_{\xi\xi\xi}^i) - \psi_\xi^i(\psi_{\eta\xi\xi}^i + \psi_{\eta\eta\eta}^i)] \quad [46]$$

and

$$\nabla^2\theta^i = A\frac{\overline{\mathrm{M}}}{\kappa^i}[\theta_\xi^i\psi_\eta^i - \psi_\xi^i\theta_\eta^i], \quad [47]$$

where the harmonic and biharmonic operators are defined as

$$\nabla^4 = \frac{\partial^4}{\partial\xi^4} + 2\left(\frac{\partial^2}{\partial\xi^2}\frac{\partial^2}{\partial\eta^2}\right) + \frac{\partial^4}{\partial\eta^4}; \quad \nabla^2 = \frac{\partial^2}{\partial\xi^2} + \frac{\partial^2}{\partial\eta^2}. \quad [48]$$

The boundary conditions at the rigid walls remain unchanged and the boundary conditions at the interfaces become:

at $\eta = Ah^{\mathrm{L}},\ 1 + Ah^{\mathrm{U}}$,

$$\psi_\eta^{-i} = \psi_\eta^{+i}; \quad \psi^{-i} = \psi^{+i} = 0; \quad \theta^{-i} = \theta^{+i} = \theta^i, \quad [49]$$

$$\psi_\xi^{-i} + h_\xi^i\psi_\eta^{-i} = \psi_\xi^{+i} + h_\xi^i\psi_\eta^{+i} = 0, \quad [50]$$

Table 1. Fluid properties

Fluids	Density (g/cm^3)	Kinematic viscosity (cm^2/s)	Dynamic viscosity (g/cm/s)	Thermal conduct. (W/cm-K)	Specific heat @ 25°C (J/g-K)	Thermal diffusivity (cm^2/s)	Coeff. of expansion (1/K)	Surface tension (dyn/cm)	Surface tension gradient (dyn/cm/K)	Pr
FC-75	1.76E + 00	8.00E − 03	1.41E − 02	6.30E − 04	1.05E + 00	3.43E − 04	1.40E − 03	1.50E + 01	−1.22E − 01	2.33E + 01
Dow 200-1.0	8.16E − 01	1.00E − 02	8.16E − 03	1.00E − 03	1.72E + 00	7.17E − 04	1.34E − 03	1.74E + 01	−6.80E − 02	1.39E + 01
Dow 200-5.0	9.13E − 01	5.00E − 02	4.57E − 02	1.17E − 03	1.72E + 00	7.48E − 04	1.12E − 03	1.97E + 01	−6.80E − 02	6.68E + 01

Table 2. Ratios of the thermophysical properties (Girifalco's $\phi = 0.75$)

Two layers	Density ratio	Kinematic viscosity ratio	Dynamic viscosity ratio	Thermal conduct. ratio	Specific heat ratio	Thermal diffusivity ratio	Coeff. of expansion ratio	Interface tension (Girifalco)	Interfacial tension gradient (Girifalco)	Pr ratio
SO 1 cSt/FC-75	0.4636	1.2500	0.5795	1.5947	1.6400	2.0903	0.9571	8.17	−0.0441	0.5980
SO 5 cSt/FC-75	0.5188	6.2500	3.2422	1.8604	1.6400	2.1796	0.8000	8.91	−0.0406	2.8675

$$-\langle p\rangle + \frac{2A}{1+h_\xi^{j2}}\langle \mu[(h_\xi^{j2}-1)\psi_{\xi\eta} - h_\xi^j(\psi_{\eta\eta}-\psi_{\xi\xi})]\rangle = \frac{h^j_{\xi\xi}}{A^3\,\overline{\mathrm{Ca}}(1+h_\xi^{j2})^{3/2}}[\sigma_0^j - A^3\bar{C}\gamma^j\theta^j] \quad [51]$$

$$\langle \mu[(1-h_\xi^{j2})(\psi_{\eta\eta}-\psi_{\xi\xi}) - 4h_\xi^j\psi_{\xi\eta}]\rangle = -\frac{\gamma^j(1+h_\xi^{j2})^{1/2}}{A}(\theta^j_\xi + h_\xi^j\theta^j_\eta) \quad [52]$$

and

$$\frac{1}{(1+h_\xi^{j2})^{1/2}}\langle \lambda[\theta^j_\eta - h_\xi^j\theta^j_\xi]\rangle = 0. \quad [53]$$

In addition to the above boundary conditions, there are the matching conditons that require the end-region solution to match the core-region solution:

$$\lim_{\xi\mapsto\infty}\psi^j(\xi,\eta) = \lim_{x\mapsto -1/2}\psi^j(x,y); \quad \lim_{\xi\mapsto\infty}\psi^j_\xi(\xi,\eta) = \lim_{x\mapsto -1/2}\psi^j_x(x,y) \quad [54]$$

and

$$\lim_{\xi\mapsto\infty}\theta^j(\xi,\eta) = \lim_{x\mapsto -1/2}\theta^j(x,y); \quad \lim_{\xi\mapsto\infty}h^j(\xi) = \lim_{x\mapsto -1/2}h^j(x). \quad [55]$$

As with the core solution, the governing field variables are expanded using the small geometric parameter A.

Solution at O(1)

Substituting the expansion into the governing equations leads to the following equation for the temperature field at $O(1)$:

$$\nabla^2\theta_0^j = 0. \quad [56]$$

The boundary conditions at the four walls are as defined previously. The boundary conditions along the interfaces and the matching conditions are as follows:

at $\eta = 0, 1$,

$$\theta_0^{-j} = \theta_0^{+j} = \theta_0^j; \quad \langle \lambda\theta_{0_\eta}\rangle = 0 \quad [57]$$

and

$$\lim_{\xi\mapsto\infty}\theta_0^j(\xi,\eta) = -\tfrac{1}{2}. \quad [58]$$

For the stream function, the governing equation at O(1) is

$$\nabla^4\psi_0^j = 0. \quad [59]$$

This equation must be solved with the interfacial boundary conditions:

at $\eta = 0, 1$,

$$\psi^{-j}_{0_\xi} = \psi^{+j}_{0_\xi}; \quad \psi^{-j}_{0_\eta} = \psi^{+j}_{0_\eta}; \quad \psi^{-j} = \psi^{+j} = 0 \quad [60]$$

and

$$\theta^j_{0_\xi} = 0; \quad h^j_{1_{\xi\xi}} = 0. \quad [61]$$

Additionally, the solution must satisfy the boundary conditions at the rigid walls, and match the core solution, which requires that

$$\lim_{\xi\mapsto\infty}\psi_0^j(\xi,\eta) = \lim_{x\mapsto -1/2}\psi_0^j(x,y) = A_0^j y^3 + B_0^j y^2 + C_0^j y + D_0^j \quad [62]$$

and

$$\lim_{\xi\mapsto\infty}\psi^j_{0_\xi}(\xi,\eta) = 0. \quad [63]$$

The only possible solution satisfying the above equation for θ_0, the boundary conditions and the matching conditions is

$$\theta_0^j = -\tfrac{1}{2}. \qquad [64]$$

The solution for the stream function must be obtained numerically. However, before proceeding to the numerical calculation, we require one additional interfacial boundary condition. This condition is obtained from the shear stress balance at the next higher order.

We proceed next to the solution for $h_1^j(\xi)$, the interfacial deformations. The governing equation is

$$h_{1\xi\xi}^j = 0. \qquad [65]$$

The boundary condition and the matching condition are:

$$h_1^j(0) = 0; \quad \lim_{\xi \mapsto \infty} h_1^j(\xi) = \lim_{x \mapsto -1/2} h_1^j(x). \qquad [66]$$

After equating the first two terms in the matching condition expansion, we find that the only possible solution for the above equation is

$$h_1^j(\xi) = 0. \qquad [67]$$

Since the governing equation for h_1^j is the same at the hot and cold ends of the cavity, in a similar fashion to above we get:

$$h_1^j(\chi) = 0. \qquad [68]$$

These two results and the matching conditions provide two conditions on the core-region solution of $h_1^j(x)$, [30], namely,

$$\lim_{x \mapsto -1/2} h_1^j(x) = \lim_{x \mapsto 1/2} h_1^j(x) = 0. \qquad [69]$$

The third condition is the conservation of volume, [20]. With these three conditions, we solve for the three unknown constants in [30]. For the solution, we obtain:

$$h_1^j(x) = \frac{\overline{\mathrm{Ca}}(\mu^{-j}A_0^{-j} - \mu^{+j}A_0^{+j})}{\sigma_0^j} x(x^2 - \tfrac{1}{4}). \qquad [70]$$

Solution at O(A)

Substituting the lower-order solutions for temperature into the governing equation leads at $O(A)$ to

$$\nabla^2 \theta_1^j = 0. \qquad [71]$$

As before, this equation must be solved with the previously defined boundary conditions at the walls and the following interfacial boundary conditions:

at $\eta = Ah_1^{\mathrm{L}}, 1 + Ah_1^{\mathrm{U}}$,

$$\theta_1^{-j} = \theta_1^{+j} = \theta_1^j; \quad \langle \lambda \theta_\eta \rangle = 0. \qquad [72]$$

Additionally, the following matching condition must be satisfied:

$$\lim_{\xi \mapsto \infty} \theta_1^j = \xi. \qquad [73]$$

The solution of [71] that satisfies the boundary and matching conditions is

$$\theta_1^j = \xi. \qquad [74]$$

In order to make the solution of ψ_1^j independent of Re, we introduce the following correlation:

$$\psi_1^j = \overline{\mathrm{Re}}\, \psi_1''. \qquad [75]$$

With this notation, the governing equation for the streamfunction at this order becomes

$$\nabla^4\psi_1^{i\prime} = \frac{1}{\nu^i}[\psi_{0_\eta}^i(\psi_{0_{\xi\eta\eta}}^i + \psi_{0_{\xi\xi\xi}}^i) - \psi_{0_\xi}^i(\psi_{0_{\eta\xi\xi}}^i + \psi_{0_{\eta\eta\eta}}^i)]. \quad [76]$$

These equations are to be solved with the wall boundary conditions, and the following boundary conditions at the interfaces:

at $\eta = Ah_1^L,\ 1 + Ah_1^U$,

$$\psi_{1_\eta}^{-j\prime} = \psi_{1_\eta}^{+j\prime}; \quad \psi_1^{-j\prime} = \psi_1^{+j\prime} = 0 \quad [77]$$

and

$$\langle\mu(\psi_{0_{\xi\xi}} - \psi_{0_{\eta\eta}})\rangle = -\gamma^j\theta_{1_\xi}^j, \quad h_{2_{\xi\xi}}^j = 0. \quad [78]$$

Using the $O(A)$ solution for θ_1^i, the shear stress balance at this order becomes

$$\langle\mu(\psi_{0_{\xi\xi}} - \psi_{0_{\eta\eta}})\rangle = -\gamma^j. \quad [79]$$

As noted earlier, this shear stress balance is a required condition for the streamfunction solution at $O(1)$.

In addition to the above boundary conditions, the following matching condition must also be satisfied:

$$\lim_{\xi\mapsto\infty}\psi_1^{i\prime}(\xi) = \lim_{x\mapsto -1/2}\psi_1^{i\prime}(x) = 0. \quad [80]$$

Here we have used results from [36]–[38] and [70]. From these results we also get

$$\lim_{\xi\mapsto\infty}\psi_{1_\xi}^{i\prime}(\xi) = 0. \quad [81]$$

The biharmonic equation [76], with the above boundary conditions and matching conditions, is solved numerically. Similar to the $O(1)$ stream function problem, before proceeding to the stream function solution at $O(A)$, we require the shear stress balance condition at the next higher order.

Next we proceed to the solution for the interfacial deformations. The governing equation and the boundary condition are:

$$h_{2_{\xi\xi}}^j = 0; \quad h_2^j(0) = 0. \quad [82]$$

Substituting the known lower-order solutions into the matching condition [55] and equating terms of the same order leads to the following solution for the above equation and boundary condition:

$$h_2^j(\xi) = -\frac{1}{2}\frac{\overline{\mathrm{Ca}}(\mu^{-j}A_0^{-j} - \mu^{+j}A_0^{+j})}{\sigma_0^j}\xi. \quad [83]$$

As before, we note that the governing equation and boundary condition at the hot and cold end walls are the same. Therefore, at the hot end-wall region, the matching condition leads to

$$h_2^j(\chi) = \frac{1}{2}\frac{\overline{\mathrm{Ca}}(\mu^{-j}A_0^{-j} - \mu^{+j}A_0^{+j})}{\sigma_0^j}\chi. \quad [84]$$

In addition, we have the conditions

$$\lim_{x\mapsto\pm 1/2} h_2^j(x) = 0. \quad [85]$$

These two conditions, together with the conservation condition,

$$\int_{-1/2}^{1/2} h_2^j(x)\,\mathrm{d}x = 0, \quad [86]$$

provide three conditions with which to obtain the unknown constants K_1^j, K_2^j and K_3^j in [40] and [41]. Solving this system of equations leads to

$$h_2^j(x) = \frac{K^j}{20}(x^2 - \tfrac{1}{4})(x^4 - x^2 + \tfrac{5}{112}), \qquad [87]$$

where

$$K^l = \overline{\mathrm{Ca}}\left[\frac{(\mu^B A_1^b - A_1^{bm})(\mu^B A_0^b - A_0^m)}{\sigma^{l^2}} - \frac{A_1^{tm}(A_0^m - \mu^T A_0^t)}{\sigma^u \sigma^l}\right] \qquad [88]$$

and

$$K^u = \overline{\mathrm{Ca}}\left[\frac{(A_1^{tm} - \mu^T A_1^t)(A_0^m - \mu^T A_0^t)}{\sigma^{u^2}} + \frac{A_1^{bm}(\mu^B A_0^b - A_0^m)}{\sigma^l \sigma^u}\right]. \qquad [89]$$

Solution at $O(A^2)$

Upon substitution of the lower-order solution, and introducing the correlation

$$\theta_2^j = \overline{M}\theta_2^{j'}, \qquad [90]$$

the governing equation for temperature at this order becomes

$$\nabla^2\theta_2^{j'} = \frac{1}{\kappa^j}\psi_{0_\eta}^j. \qquad [91]$$

The boundary conditions at the walls are as before, and at the interfaces we have:
at $\eta = Ah_1^L + A^2h_2^L,\ 1 + Ah_1^U + A^2h_2^U$,

$$\theta_2^{-j'} = \theta_2^{+j'} = \theta_2^{j'}; \quad \langle \lambda\theta_{2_\eta}' \rangle = 0. \qquad [92]$$

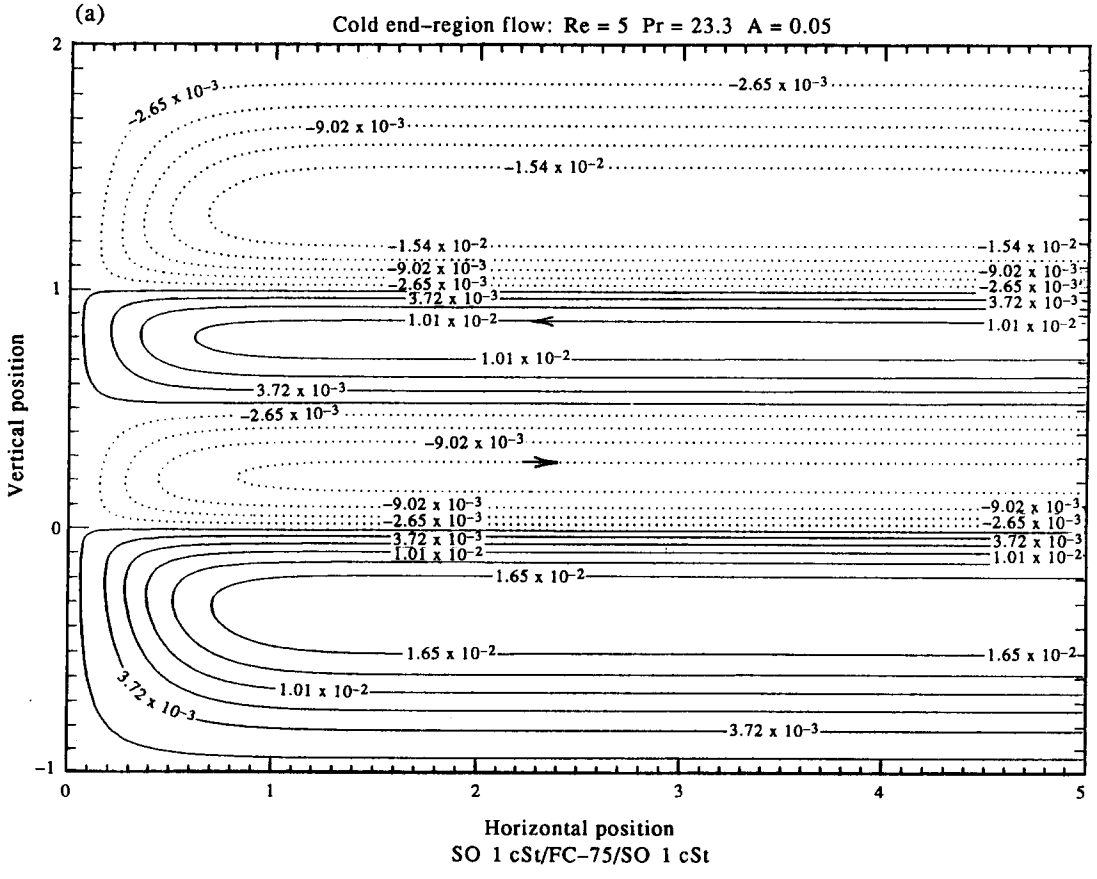

Figure 2(a). *Caption on p. 409.*

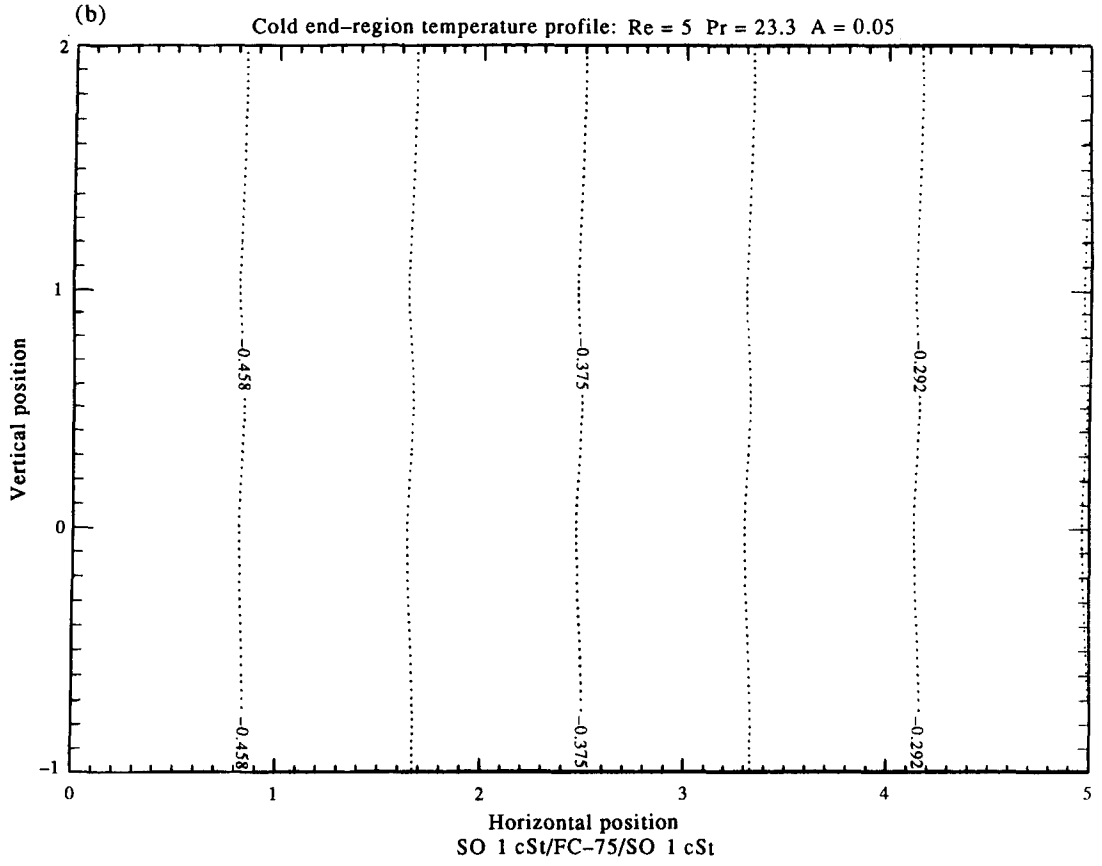

Figure 2(b). *Caption* opposite.

The matching condition is

$$\lim_{\xi \mapsto \infty} \theta_2^{i\prime} = \frac{1}{\kappa^i}\left(\frac{A_0^i}{4}\eta^4 + \frac{B_0^i}{3}\eta^3 + \delta_1^i\eta + \delta_2^i\right). \qquad [93]$$

For computational convenience, rather than imposing this matching condition, we impose the following equivalent condition instead:

$$\lim_{\xi \mapsto \infty} \theta_{2_\xi}^{i\prime} = 0. \qquad [94]$$

The harmonic problem with the above prescribed boundary conditions is solved numerically.

As noted earlier, we require the shear stress balance condition at this order to solve the $O(A)$ stream function problem. This condition is

$$\langle \mu(\psi'_{1_{\xi\xi}} - \psi'_{1_{\eta\eta}})\rangle = -\Pr\gamma^i\theta_{2_\xi}^{i\prime}. \qquad [95]$$

Numerical Modeling

The finite-difference method is used to solve the harmonic and the biharmonic problems. The harmonic problem is discretized using a 5-point operator providing $O(\delta^2)$ accuracy, while the biharmonic problem is discretized using a 13-point operator. The mesh is stretched along the horizontal (x)-direction using an exponential function, and it is stretched along the vertical (z)-direction using a cosine function in each layer. IMSL routines are used to solve the resulting linear system of equations.

The end region is horizontally extended towards the core a distance 5 times the middle-layer height. Therefore, the computational domain in non-dimensional space is 5.0 (horizontal) by $1 + d^B + d^T$ (vertical). The mesh resolution in each layer is 51 × 51. Further refinement of the mesh was found to have an insignificant influence on the results.

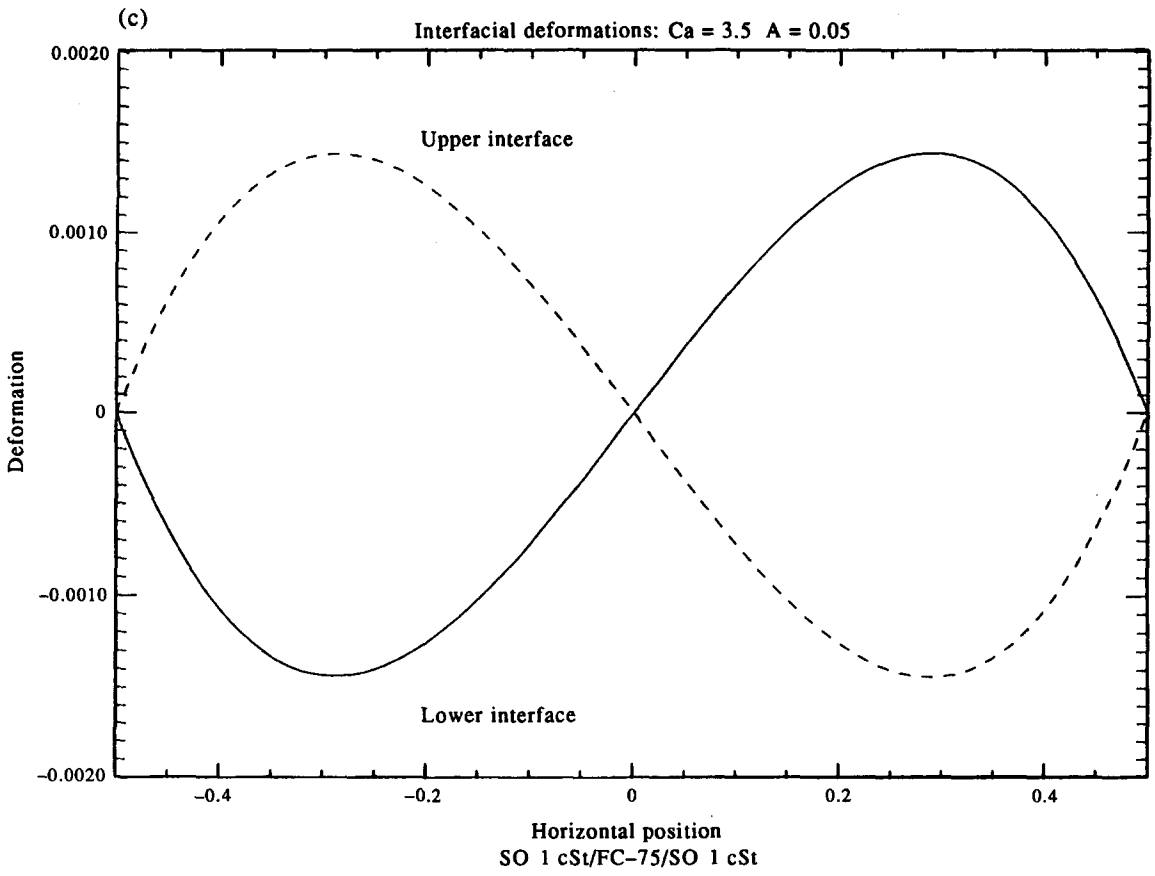

Figure 2(c)

Figure 2. Symmetric encapsulation—equal layer heights, $A = 0.05$, Re = 5: (a) cold end-region flow correct up to $O(A^2)$; (b) temperature field in the cold end region correct up to $O(A^3)$; (c) interfacial deformations correct up to $O(A^3)$.

RESULTS

Thermocapillary convection in three immiscible layers in a shallow cavity is characterized by 15 parameters. These are the 8 ratios of the thermophysical properties, and the height ratios of the upper and lower layers with respect to the middle layer, the aspect ratio, the Re and Pr of the middle layer, the interfacial tension, and interfacial tension gradient ratios of the upper interface with respect to the lower interface and the lower interface Ca.

For the purpose of this investigation, we select two systems. These are composed of fluorinert FC-75 liquid, encapsulated above and below by two different silicone oils (SO; 1 and 5 cSt). The thermophysical properties of these liquids are listed in table 1. We select two combinations: (i) SO 1 cSt/FC-75/SO 1 cSt; and (ii) SO 1 cSt/FC-75/SO 5 cSt. The ratios of the thermophysical properties for these systems are listed in table 2. As the interfacial tension and interfacial tension gradient data for these systems are unavailable in the literature, a method proposed by Girifalco & Good (1957) is used to estimate the interfacial tension based on the surface tension of the adjacent liquids. For both cases considered, the interfacial tension gradient is negative.

Case (i) represents the encapsulation of the middle layer (FC-75) liquid with "equal" viscosity liquid—the *symmetric encapsulation* case; and case (ii) represents encapsulation by different viscosity liquids, one encapsulant layer being 5 times more viscous than the other—the *non-symmetric encapsulation* case. Neither of these systems can be realized in terrestrial gravity, although they are of interest for studying pure thermocapillary flow under zero-gravity conditions.

First we consider the *symmetric encapsulation* case when all three layers are of "equal" viscosity and equal height, case (i). The flow streamlines for this case, correct to $O(A^2)$, are shown in figure 2(a). Symmetric interfacial tension gradients produce counter-rotating rolls in the middle layer. At both interfaces, liquid is pulled towards the cold wall. The flow in the upper and lower encapsulant layers is mirror-symmetric. The temperature field, correct to $O(A^3)$, is shown in figure 2(b). For the aspect ratio and Re chosen, the temperature field depicts a nearly conductive state in all three layers. The interfacial deformations, correct to $O(A^3)$, are shown in figure 2(c). The deformations are perfectly symmetric about the center of the cavity. Similar to S&D's single layer, the middle layer bulges near the cold wall and contracts near the hot wall.

The middle-layer flow in the above case is weaker than flow in an unencapsulated free–free layer, as evidenced by comparing the non-dimensional maximum leading-order stream function values in the core region. The maximum leading-order stream function value for an unencapsulated free–free layer obtained from S&D is 1.6×10^{-2}. The maximum value for the above encapsulated case is 1.3×10^{-2}. The influence of encapsulation on reducing the middle-layer flow is more significant with higher viscosity encapsulants.

Next we consider the *symmetric encapsulation* case (i) when encapsulant layers are one-quarter the thickness of the middle layer. For this case, the flow streamlines, correct to $O(A^2)$, are shown in figure 3(a). The flow pattern and temperature distributions are qualitatively unchanged. The flow in all three layers is slower than when all layers are of equal height. Reducing the encapsulant layer heights further will lead to even slower flow in all three layers. This is attributed to increased viscous resistance to flow in the encapsulant layers as the layer thickness is reduced. The limiting case of zero encapsulant layer thicknesses will lead to near suppression of the middle-layer flow as a rigid boundary condition is approached. It is worth noting, however, that the asymptotic analysis becomes invalid as the height ratios approach $O(A)$. In this limit the aspect ratio of the encapsulant

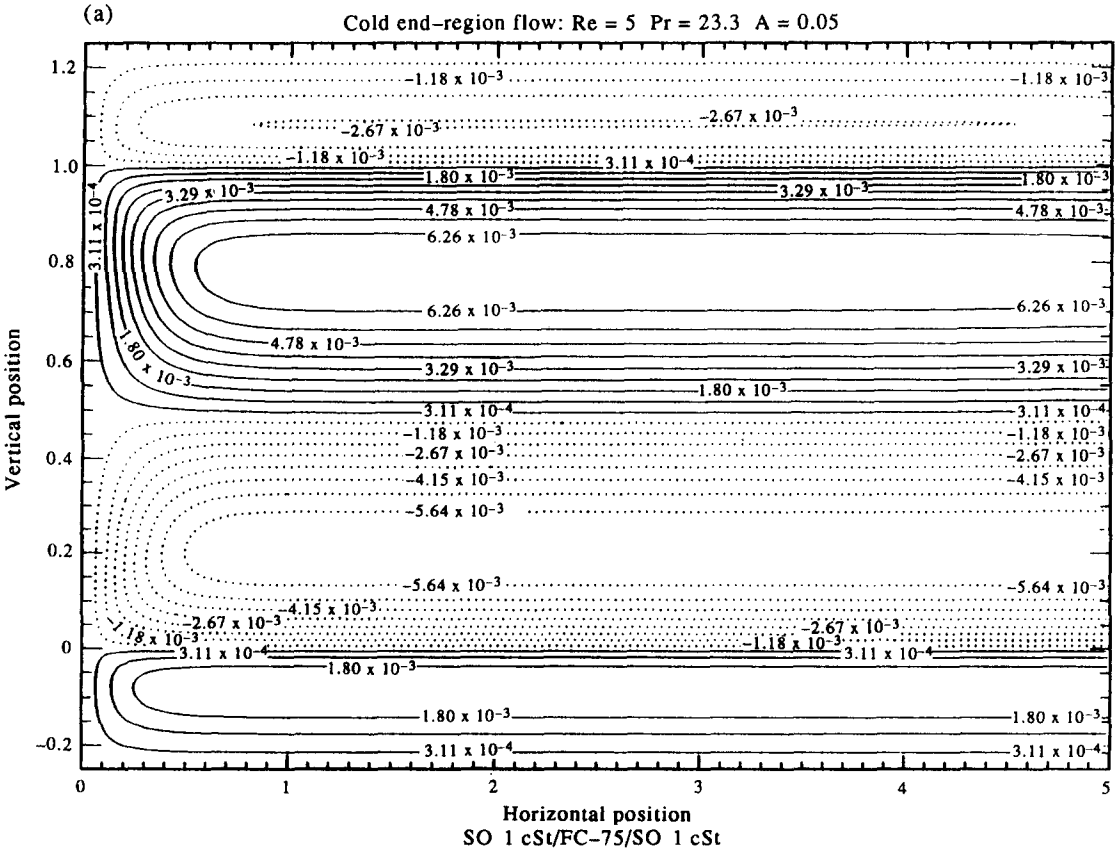

Figure 3(a). *Caption opposite.*

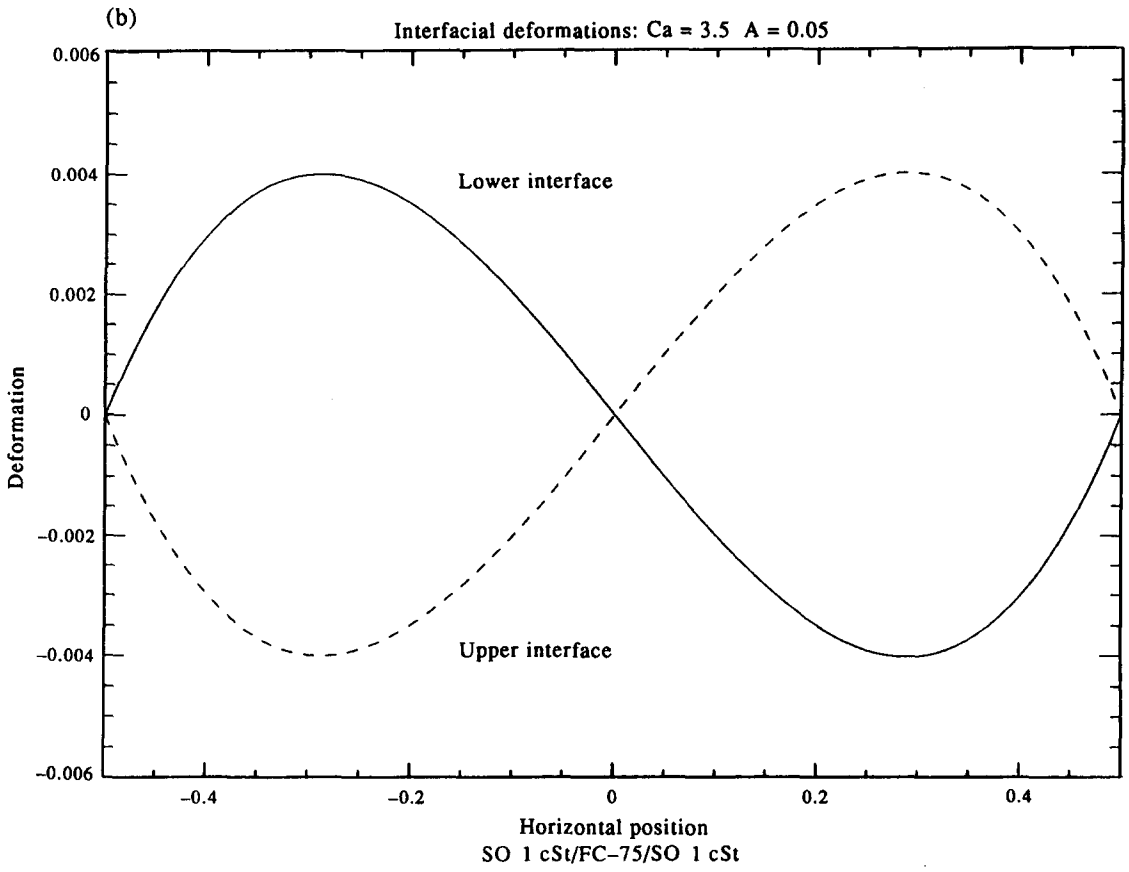

Figure 3(b)

Figure 3. Symmetric encapsulation—unequal layer heights, $A = 0.05$, Re = 5: (a) cold end-region flow correct up to $O(A^2)$; (b) interfacial deformations correct up to $O(A^3)$.

layers approaches $O(A^2)$, and the velocity scale in the encapsulants becomes an order of magnitude less than in the middle layer.

The interfacial deformations for the above *symmetric* case (i) with unequal layer heights are shown in figure 3(b). Here we notice a dramatic difference compared to the case of equal layer heights. The middle layer contracts near the cold end wall and bulges near the hot wall. This is in contrast to the equal layer heights case, where the middle layer bulges near the cold wall and contracts near the hot wall. The deformation of the interface is due to the local dynamic pressure difference across the interface. When encapsulant layers are thinner than the middle layer, the local dynamic pressure near the cold wall in the encapsulant layers becomes larger than in the middle layer, forcing the interface to bend into the middle layer. The opposite occurs near the hot wall. This, however, is valid only as long as the ratio of the encapsulant layer height to the middle layer height is of $O(1)$ and does not approach $O(A)$.

For the *non-symmetric encapsulation* case with equal height layers, the flow streamlines, correct up to $O(A^2)$, are shown in figure 4(a). In the middle layer, the flow is no longer symmetric. It is still composed of two counterrotating roll cells. The vertical extent of the upper roll cell is significantly smaller than the lower roll. The flow in the upper, more viscous encapsulant, is significantly weaker than in the lower encapsulant. This is despite the fact that the interfacial tension gradients at both interfaces are the same. The interfacial deformations at the two interfaces correct to $O(A^3)$ are shown in figure 4(b). The deformation at the upper interface, which has the larger interfacial tension, is significantly smaller than at the lower interface. Consistent with the *symmetric encapsulation* case, the middle layer bulges near the cold wall and contracts near the hot wall. Therefore, near the cold wall, the local dynamic pressure is higher in the middle layer than in the more viscous upper encapsulant and in the lower encapsulant. The temperature field is very

similar to that for the *symmetric encapsulation* case and also represents a more or less conductive state.

We also considered the *non-symmetric encapsulation* case, where encapsulant layers are one-quarter as thick as the middle layer. As with the *symmetric encapsulation* case, the middle layer in this case contracts near the cold end wall and bulges near the hot wall. This also is in contrast to the *non-symmetric encapsulation* case with equal layer heights.

CONCLUSION

Thermocapillary flow in multiple immiscible liquid layers confined in a differentially heated shallow cavity with rigid and insulated upper and lower boundaries is investigated. Sen & Davis (1982) applied the method of matched asymptotic expansions to determine thermocapillary flow in a single liquid layer in a differentially heated shallow cavity. This method is extended to investigate thermocapillary flow in a three-layer immiscible liquid system featuring two deformable interfaces.

With *symmetric encapsulation* and equal layer heights, the flow in the middle layer is qualitatively the same, but weaker than in S&D's single layer. However, when the encapsulant thickness is much less than that of the middle layer, interfacial deformations, and thereby flow in the encapsulated layer, are no longer the same as in the unencapsulated layer. Rather than bulging near the cold wall, the middle layer contracts near the cold wall and bulges near the hot wall. The influence of mechanical coupling between the layers is also quite apparent with *non-symmetric encapsulation*, which leads to unequal size rolls.

Although, the parameters used in this study are not directly applicable to crystal growth applications, the results of this analysis indicate that: (1) liquid encapsulation has the potential for reducing thermocapillary convective flow in the middle (melt) layer; and (2) the flow pattern in the

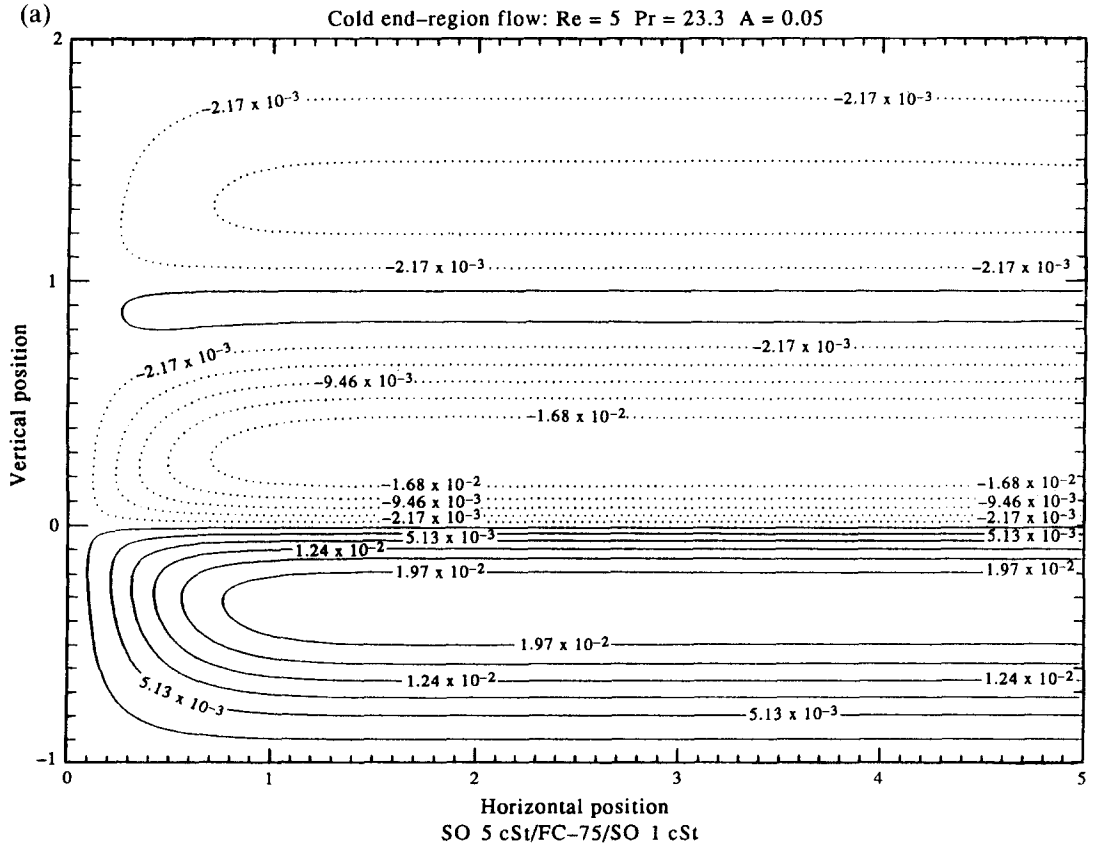

Figure 4(a). *Caption opposite.*

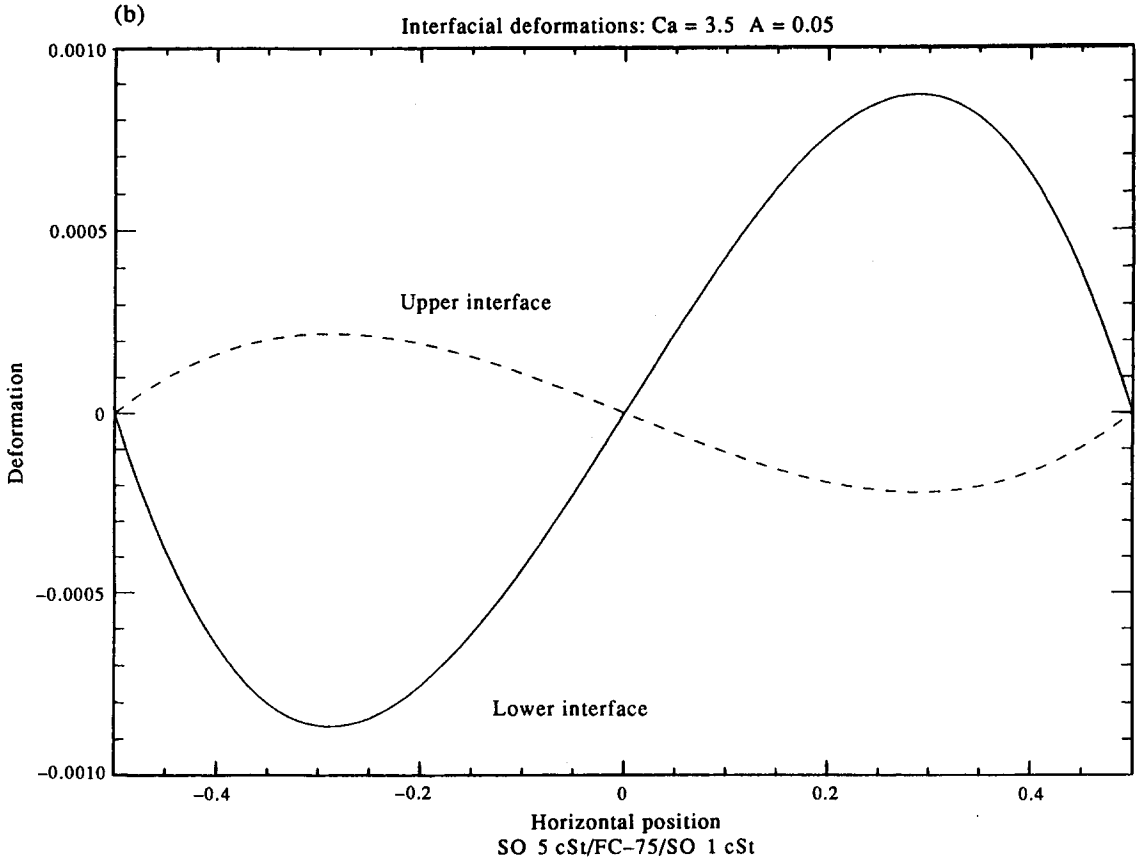

Figure 4(b)

Figure 4. Non-symmetric encapsulation—equal layer heights, $A = 0.05$, Re = 5: (a) cold end-region flow correct up to $O(A^2)$; (b) interfacial deformations correct up to $O(A^3)$.

encapsulated layer depends on the encapsulation thickness and the thermophysical properties of the encapsulants.

Acknowledgement—Support from NASA MSAD, under Grant NAG3-1094, for this study is greatly appreciated.

REFERENCES

BAROCELA, E. & JALILEVAND, A. 1987 Liquid encapsulated float zone method for microgravity production of gallium arsenide. AIAA paper 87-0390.

BIRIKH, R. V. 1966 Thermocapillary convection in a horizontal layer of liquid. *Appl. Mech. Tech. Phys.* **7**, 43–44.

CORMACK, D. E., LEAL, L. G. & IMBERGER, J. 1974 Natural convection in a shallow cavity with differentially heated end walls, part I. Asymptotic theory. *J. Fluid Mech.* **65**, 209–229.

DOI, T. & KOSTER, J. N. 1993 Thermocapillary convection in two immiscible liquid layers with free surface. *Phys. Fluids A: Fluid Dynam.* **5**, 1914–1927.

FONTAINE, J.-P. & SANI, R. L. 1992 High Prandtl number fluids in a multilayered system under 1-g or μ-g environment. Report ESA SP-333, pp. 197–202.

GIRIFALCO, L. A. & GOOD, R. J. 1957 A theory for the estimation of surface and interfacial energies—I. Derivation and application to interfacial tension. *J. Phys. Chem.* **61**, 904–909.

LEVICH, V. G. 1962 *Physicochemical Hydrodynamics*. Prentice–Hall, Englewood Cliffs, NJ.

PRAKASH, A., FUJITA, D. & KOSTER, J. N. 1993 Surface tension and buoyancy effects on a free–free layer. *Eur J. Mech. B/Fluids* **12**, 15–29.

PRAKASH, A. & KOSTER, J. N. 1993 Natural and thermocapillary convection in three layers. *Eur. J. Mech. B/Fluids* **12,** 635–655.

PRAKASH, A. & KOSTER, J. N. 1994 Convection in multiple layers of immiscible liquids in a shallow cavity—I. Steady natural convection. *Int. J. Multiphase Flow* **20,** 383–396.

SEN, A. & DAVIS, S. H. 1982 Steady thermocapillary flows in two-dimensional slots. *J. Fluid Mech.* **121,** 163–186.

VILLERS, D. & PLATTEN, J. K. 1990 Influence of interfacial tension gradients on thermal convection in two superposed immiscible liquid layers. *Appl. Scient. Res.* **47,** 177–191.